




High degree of N-functionalization in macroscopically assembled carbon nanotubes

Ruairi J. McGlynn¹, Paul Brunet¹, Supriya Chakrabarti¹, Adam Boies², Paul Maguire¹, and Davide Mariotti^{1,*} 

¹Nanotechnology and Integrated Bio-Engineering Centre (NIBEC), Ulster University, Newtownabbey BT37 0QB, UK

²Department of Engineering, University of Cambridge, Cambridge CB2 1PZ, UK

Received: 1 February 2022

Accepted: 18 June 2022

Published online:
15 July 2022

© The Author(s) 2022

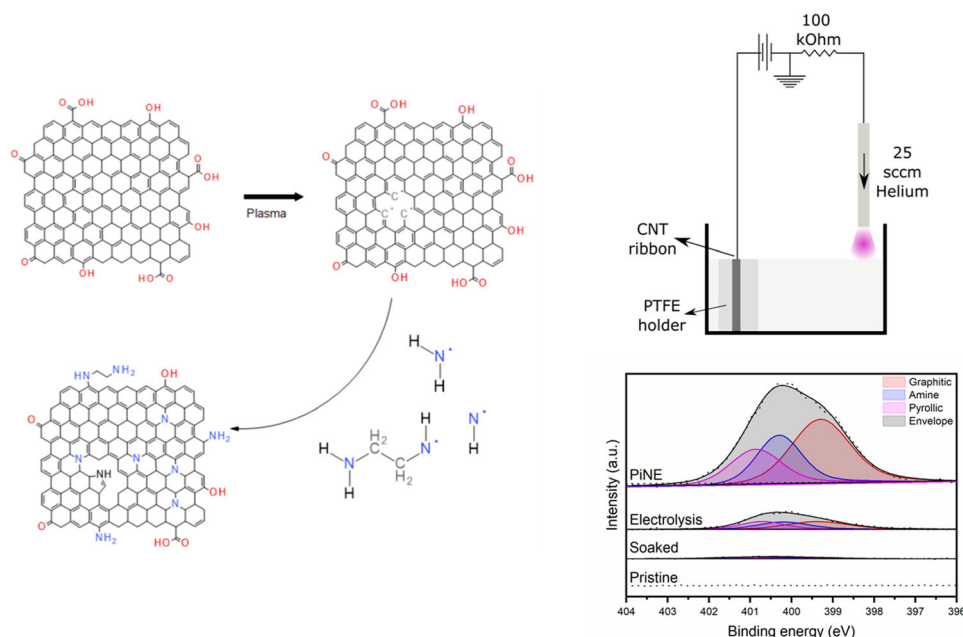
ABSTRACT

Nitrogen doping of carbon nanomaterials has emerged as a method to develop novel material properties, though limitations in the form of extended treatment times, harsh chemical usage and limited total nitrogen content exist. Here, macroscopic ribbon-like assemblies of carbon nanotubes are functionalized with nitrogen using a simple direct current-based plasma–liquid system. This system utilizes the plasma-generated species in an ethanol:water solution with ethylenediamine as a nitrogen precursor for the nitrogen functionalization of the carbon nanotube assembly. These unique, plasma-generated species and pathways enable rapid and high levels of functionalization with the atomic concentration of nitrogen reaching 22.5%, with amine groups, pyrrolic groups and graphitic nitrogen observed in the X-ray photoelectron spectra, the highest ever achieved. This nitrogen content is demonstrated to be significantly higher than a comparative electrolysis process. This demonstrates that this plasma process enhances the availability of nitrogen from the ethylenediamine precursor, facilitating greater functionalization.

Handling Editor: Dale Huber.

Address correspondence to E-mail: d.mariotti@ulster.ac.uk

GRAPHICAL ABSTRACT



Introduction

Modification of carbon nanotubes (CNT) to produce advanced functional materials is of high industrial interest and can be achieved in a range of ways, which can include modifying the individual CNT as well as modifying the bulk application material. For instance, in the latter case, great improvements have been achieved by densification with record performance parameters [1]. When individual CNT are the target of modification, two primary approaches are generally considered to enhance and optimize application-relevant properties. The first option is to create CNT-based composites by depositing another material, such as transition metals or their oxides, onto the surface of the CNT to develop new properties, often relevant to electrical [2] or electronic applications [3–6]. The alternative, and the focus of this work, is to functionalize the CNT with chemical species to yield different material properties.

Replacing carbon atoms in the CNT lattice with oxygen, nitrogen or boron has generated significant interest and attention for modifying the electronic

and chemical properties of CNT. For example, due to their high surface energy, individual CNT tend to agglomerate which can limit the efficacy of their utilization in some real-world products. Covalent functionalization of the CNT sidewalls with oxygen-based or nitrogen-based functional groups can be used to modify the surface energy of the CNT [7], and in doing so the inherent hydrophobic nature of CNT can be reduced. This improves the wettability and dispersibility in solvents, by reducing the tendency of the CNT to agglomerate. This is critical in applications where preserving the long-term dispersibility of CNT in liquid is of paramount importance, such as for solar-thermal energy conversion [8–11]. Also, in other applications surface-functionalized CNT have been utilized to overcome the issue of poor interfacial interaction between CNT and epoxy matrix when forming composites, reducing the probability of delamination failure and enhancing the mechanical properties [12, 13].

Introducing nitrogen functional groups into the graphitic lattice is also of interest for a range of energy storage devices, where this can produce faradaic pseudocapacitive reactions which are of appeal

in supercapacitor applications [14]. Small concentrations of nitrogen in double-walled CNT (0.86 at%) have been shown to reduce the charge transfer resistance (threefold) and almost doubling the specific capacitance [15]. The increase of the specific capacitance of multi-walled CNT (MWCNT) has been ascribed to the introduction of pyridinic and pyrrolic functional groups as well as the increase in the structural disorder [16]. Battery technologies could also benefit from the integration of N-doped carbon materials, particularly pyridinic nitrogens, which have been found to anchor lithium-polysulfide complexes, therefore improving the cyclic performance [17, 18]. N-doped carbons have recently been demonstrated to work as an alternative catalyst material, and presents a much less expensive alternative to Pt [19]. N-doped graphene (4 at%) have not only been demonstrated to act as a catalyst for the oxygen reduction reaction, but they also are insensitive to the poisoning by carbon monoxide. The high electrocatalytic activity and stability of N-doped graphene have been shown to be vastly superior to Pt [20]. Alternatively, arrays of N-doped CNT have been demonstrated to a current density of almost 4 times that of a Pt/C electrode, with stability of up to 100,000 cycles [21]. Amino-groups functionalized CNTs have been demonstrated as high-rate and highly cyclable capacitors, benefiting from double-layer capacitance due to the hydrophobicity but also strong pseudocapacitance from the increase active sites for redox reactions [22]. Further, amine-functionalized CNTs have been demonstrated to have hydrogen evolution and oxygen evolution reactions with efficacies comparable to traditional metal-based electrocatalysts and strong stability [23]. It is clear that a wealth of applications can be enhanced depending on the predominant functional groups.

A variety of methods have been used to produce nitrogen-doped CNT, both by the addition of a nitrogen precursor to the CNT growth process and as a post-synthesis step. Replacing hydrogen with a nitrogen-containing alternative in a chemical vapor deposition reaction is a popular option to fabricate N-doped CNT as they grow. A variety of doping levels have been achieved with ammonia (0.86–7.3 at%) [15, 24–26] acetonitrile (4 at%) [27], acrylonitrile (7.5 wt%) [28] or imidazole (13.82 wt%) [29]. By milling pre-fabricated CNT with melamine or urea (0.6 g:0.26 g) for 4 h and subsequently annealing at 600 °C for 1 h in a nitrogen environment, CNT with a

nitrogen content of up to 9.6 wt% could be produced [30]. Gas-phase nitrogen-based plasmas have also displayed the capability of generating functional groups on the sidewalls of MWCNT [16]. A total atomic nitrogen concentration of 21.26% was achieved, comprised of pyridine, pyrrole, quaternary nitrogen, pydrinic-N-oxide and nitrogen–oxygen groups. It appears that achieving high-doping contents of CNTs with nitrogen groups is also more difficult than other carbon allotropes as highlighted in 2016 [31], where 36.38 at% and 29.82 at% nitrogen doping could be achieved for graphene quantum dots and graphene, respectively. However, only 7.79 at% could be doped into CNTs using the same methods.

In this work, the functionalization of macroscopic assemblies of CNT, referred to herein as “ribbons”, by a simple, single-step atmospheric-pressure plasma-liquid treatment is investigated. Atmospheric pressure plasmas have been shown in the literature to produce a range of radicals and species when interacting with the surface of a solution [32]. Whilst some of these are short-lived and go on to produce other species, here we have found that the plasma-liquid treatment enhances functionalization of the CNT over electrolysis. Ethylenediamine (EDA) is added to the electrolyte solution as a nitrogen source as it has previously been demonstrated to be effective in the preparation of N-doped carbon quantum dots [33, 34]. The ribbon electrode configuration reported in this manuscript was developed and selected following various trials with different mounting configurations (see supporting information for more details). The reaction steps for the decomposition of EDA by plasma-generated species are also discussed.

Experimental methodology

Synthesis of the carbon nanotube ribbons

The carbon nanotube ribbons in this work are produced by direct-spinning from a floating-catalyst chemical vapor deposition system [35–37]. The iron catalyst nanoparticles are formed by the thermal decomposition of ferrocene vapor carried in a carrier gas of hydrogen. Sulfur is a critical precursor for this reaction, therefore thiophene is transported in the carrier gas stream through the furnace. The hydrogen carrier gas also helps to maintain the catalytic activity

of the iron particles by etching amorphous carbon coatings [38]. After several minutes of flowing the ferrocene and thiophene, hydrocarbons are added to the furnace in the form of methane [39]. After the hot zone of the furnace, the material begins to cool and a dense web of dark carbon material forms in the center of the work tube. This aerogel is sufficiently strong that it can be drawn out to form a long black “sock”.

To produce the CNT ribbons in this work, gas flows of 116 standard cubic centimeters per minute (sccm) of hydrogen through the ferrocene bubbler, 90 sccm of hydrogen through the thiophene bubbler, a methane flow rate of 160 sccm and a carrier hydrogen flow rate of 1470 sccm are flown through a tube furnace held at 1290 °C. The materials are processed by pressing the aerogel into “ribbons” as described in the supporting information. For compressing the aerogel intertube distance [1, 40]. Secondly, this morphology allows for a more rigorous and repeatable functionalization process to take place as well as a more reliable characterization that would allow comparing different samples.

Plasma-induced non-equilibrium electrochemistry process

The CNT ribbons are then treated by a plasma-induced non-equilibrium electrochemistry process (PiNE), see Fig. 1a–c. An electrolyte solution of 1:9 ethanol:distilled water is mixed with ethylenediamine as the nitrogen precursor. Ethylenediamine was selected specifically as it had previously been successfully utilized to generate nitrogen doped carbon quantum dots in a similar configuration of the PiNE system [33]. Three different concentrations of ethylenediamine are explored, 2.5 volume percent (vol%), 5 vol% and 10 vol%, with the total electrolyte volume maintained at 18 mL to fully submerge the CNT ribbon. The CNT ribbon is secured within a polytetrafluoroethylene (PTFE) holder (Fig. 1b, c) and connected as the anode. The process may also induce oxidation at the surface of the CNTs via hydroxyl species produced by the plasma at the interface. This is observed by an increase of oxygen concentration also for solutions without EDA. The atmospheric-pressure plasma discharge is used at the cathode and was sustained within a helium gas flow of 25 sccm (“PiNE”, Fig. 1a). The discharge was sustained for 10 min at a set constant current of 10 mA. The plasma

discharge was initiated at 1.43 kV and through the process it varied within a small range of voltage values (1.36–1.45 kV). The configuration for the PiNE treatment was the result of an optimization process and other methodologies were also trialed (see Supporting Information). The CNT ribbons, after PiNE treatment, were then rinsed three times with distilled water ($3 \text{ M}\Omega \text{ cm}^{-1}$) to remove any remaining electrolyte. To compare the PiNE treatment, the pristine samples were also treated by soaking, where the sample is simply submerged in the electrolyte solution (referred to as “soaked”, Fig. 1d) for 10 min. A second comparative process was performed through electrolysis (“electrolysis”, Fig. 1e). For the electrolysis method, the CNT ribbon was also secured with the same PTFE holder (Fig. 1b, c) and connected as the anode, with a 1 cm^2 piece of platinum foil acting as the counter-electrode. A 10 mA of constant current is sustained for 10 min of treatment. The voltage applied was started and maintained at 1 kV for the time of the treatment. The same rinsing procedure was followed whereby the CNT ribbons were rinsed three times with distilled water ($3 \text{ M}\Omega \text{ cm}^{-1}$) to remove any remaining electrolyte after the soaking and electrolysis treatments. The comparative experiments, soaking and electrolysis, were carried out only at the highest concentration of EDA.

For each of these processes, four separate samples are treated for each concentration, with the mean and standard deviation generated as a measure of the variance within the process.

Experimental details

To prepare samples for scanning electron microscopy (See supporting information), Raman and X-ray photoelectron spectroscopy (XPS) the ribbons are laid down onto a silicon substrate. Several drops of ethanol are applied and evaporated via a hotplate set at 70 °C, resulting in a dry ribbon that is adhered to the silicon substrate. A Schottky field emission Hitachi SU5000 instrument with an X-Max^N 80 silicon drift detector from Oxford Instruments is used to assess the thickness of the CNT ribbons. The samples are then attached to the sample stub by double-sided conductive carbon or copper tape which also acts to ground the sample. EDX measurements were consistently taken during the SEM measurements, at 10 kV, with a spot intensity of 50 and a working distance of 10 mm.

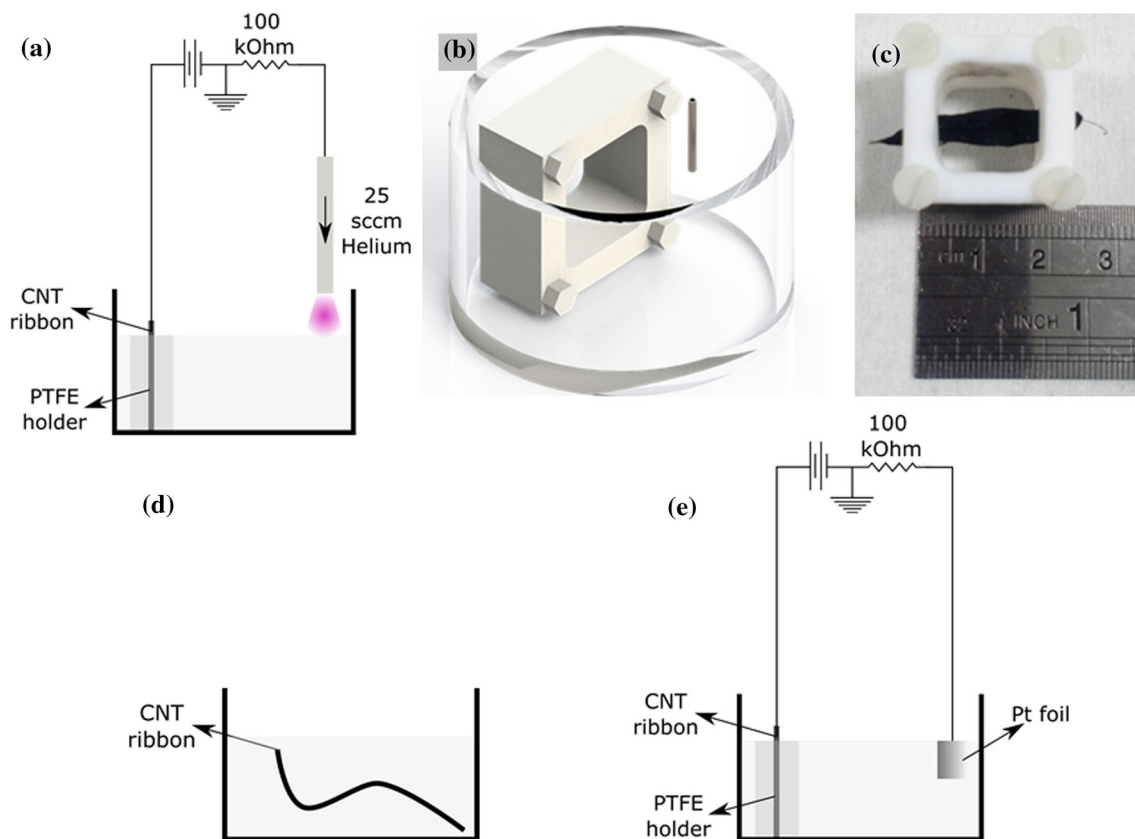


Figure 1 Schematic diagrams of the configurations used to treat the carbon nanotube ribbons in this work. **a–c** Show these schematic, a 3D render of positioning and the securing the CNT in

the PTFE for PiNE processing. Schematics **d** and **e** illustrate the Soaking and Electrolysis configurations respectively.

Raman measurements were obtained with a Horiba LabRAM 300 spectrometer. A helium–neon laser is used to produce a fixed wavelength light beam of 632.81 nm, which is incident onto the sample. Five measurements were made across the length of the produced CNT ribbons, approximately 0.5 cm apart to both enable characterization of the graphitization of the material and the variation within the sample. The data was baseline corrected with an eighth-order polynomial baseline subtraction by the system software (LabSpec, Horiba). The areas enclosed by each component in the spectra were calculated by integrating with OriginPro 8.5 software. The D band was considered the peak at 1335 cm^{-1} with the G band at 1580 cm^{-1} . A third peak at 1622 cm^{-1} was considered as the D' band and was fitted to exclude it from the G band area. The areas of the D and G band peaks are calculated using Origin software.

XPS was carried out with a Kratos Axis Ultra DLD spectrometer. The X-ray source was an Al anode

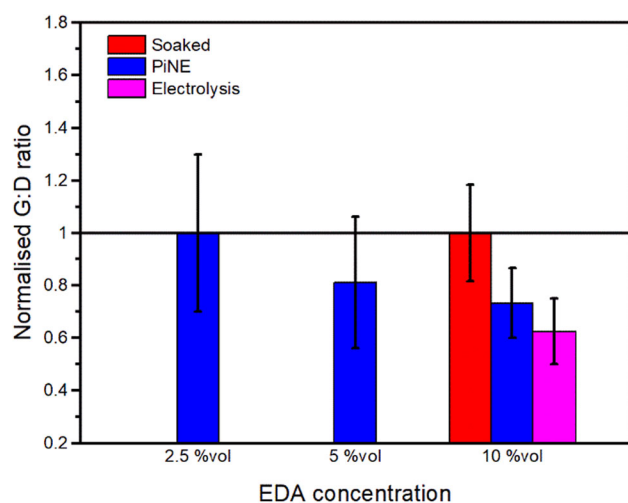
(1486.7 eV), and the operating pressure of the system was maintained at 10^{-9} bar. High-resolution spectra scans were carried out with a resolution of 0.05 eV . The C 1 s high-resolution spectra were de-convoluted, and the adventitious carbon C–C peak was charge corrected to 284.8 eV . Shirley backgrounds were fitted to the dataset for each high-resolution spectrum. As the samples were sufficiently conductive to prevent sample charging, no additional grounding between the sample and sample bar was used. The conductive nature of the samples made the use of the neutralizer beam redundant, reducing the number of simultaneous interactions with the sample.

Table 1 The data sets used to calculate the normalized values for conductivity, cross-sectional area and g-band to d-band area ratios

EDA concentration (vol%)	G:D ratio	
	Pristine	After treatment
<i>PiNE</i>		
2.5	1.0 ± 0.2	1.0 ± 0.3
5	1.6 ± 0.2	1.3 ± 0.4
10	1.5 ± 0.2	1.1 ± 0.2
<i>Soaked</i>		
10	1.1 ± 0.3	1.1 ± 0.2
<i>Electrolysis</i>		
10	0.8 ± 0.2	0.5 ± 0.1

Results and discussion

Raman spectroscopy was performed to determine the G:D ratios by dividing the peak area for the G-band by the peak area for the D-band. These were calculated for the samples before and after the treatment to illustrate any change in the defect concentration, with the mean values plus or minus one standard deviation reported in Table 1. To note that due to the variability of the CNT synthesis method, the *pristine* ribbons presented slightly different G:D ratios. In order to account for this variability and compare the samples, the G:D ratio for the treated sample is

**Figure 2** The normalized Raman G band to D band ratio for carbon nanotube ribbons treated in a solution containing ethylenediamine in varying concentrations. The measured G:D ratios of the samples after treatment were normalized against the G:D ratio measured prior to the treatment, i.e. divided by the pristine values as per Table 1.

normalized to the G:D area ratio of the pristine sample, presented in Fig. 2. Therefore, a value greater than 1 suggests an increase in the graphitization, whilst a normalized G:D value lower than 1 suggests an increase in disorder of the graphitic lattice by means of increased defect content. The sample treated with PiNE at 2.5%vol EDA shows no significant change in the G:D ratio over the pristine sample counterparts. At both 5%vol and 10%vol EDA a 19% and 27% diminishment of the G:D ratio is observed for the PiNE samples, respectively. However, the largest G:D decrease is observed for the electrolysis samples, where a 37.5% decrease in G:D ratio was observed compared to the same samples prior to treatment. Given that there is a decrease in the G:D ratio for the PiNE samples at 5%vol and 10%vol EDA, it is expected that nitrogen has grafted into the graphitic lattice. If multiple carbon atoms had been replaced with a single nitrogen atom, or if the carbon-carbon double bonds of the graphitic lattice have opened to accept additional functional groups or indeed other defective-type functionalizations, the CNT wall structure will be altered, explaining the diminished G:D ratio observed. The soaked sample appears to be unaffected, as it would be expected when no chemical reactions are promoted.

X-ray photoelectron spectroscopy is utilized to determine the degree and type of nitrogen inclusion within the graphitic lattice of the CNT. In order to analyze the type of functional group bonds to the CNT, upper and lower limits were set for the peak position of each functional group type including amine, graphitic, pyridinic, pyridinic-N oxide and pyrrolic (Supporting information Table S1) and the peak areas were calculated by the CasaXPS software. However based on our initial analysis it was clear that the contributions of pyridinic and pyridinic-N oxide were negligible, hence these were omitted from subsequent fitting and only amine, graphitic and pyrrolic are considered in the analysis below.

The pristine samples prior to any treatment did not show any nitrogen peak. PiNE samples are compared for 2.5 vol%, 5 vol% and 10 vol% EDA concentration, Fig. 3a. Of the considered bonding types, only three appear to be present, amines groups, pyrrolic groups and graphitic groups. It is blatantly obvious that nitrogen functional groups have been introduced following PiNE. In addition, Fig. 3b compares the nitrogen peak after soaking, electrolysis and PiNE treatment with 10 vol% EDA, with the pristine

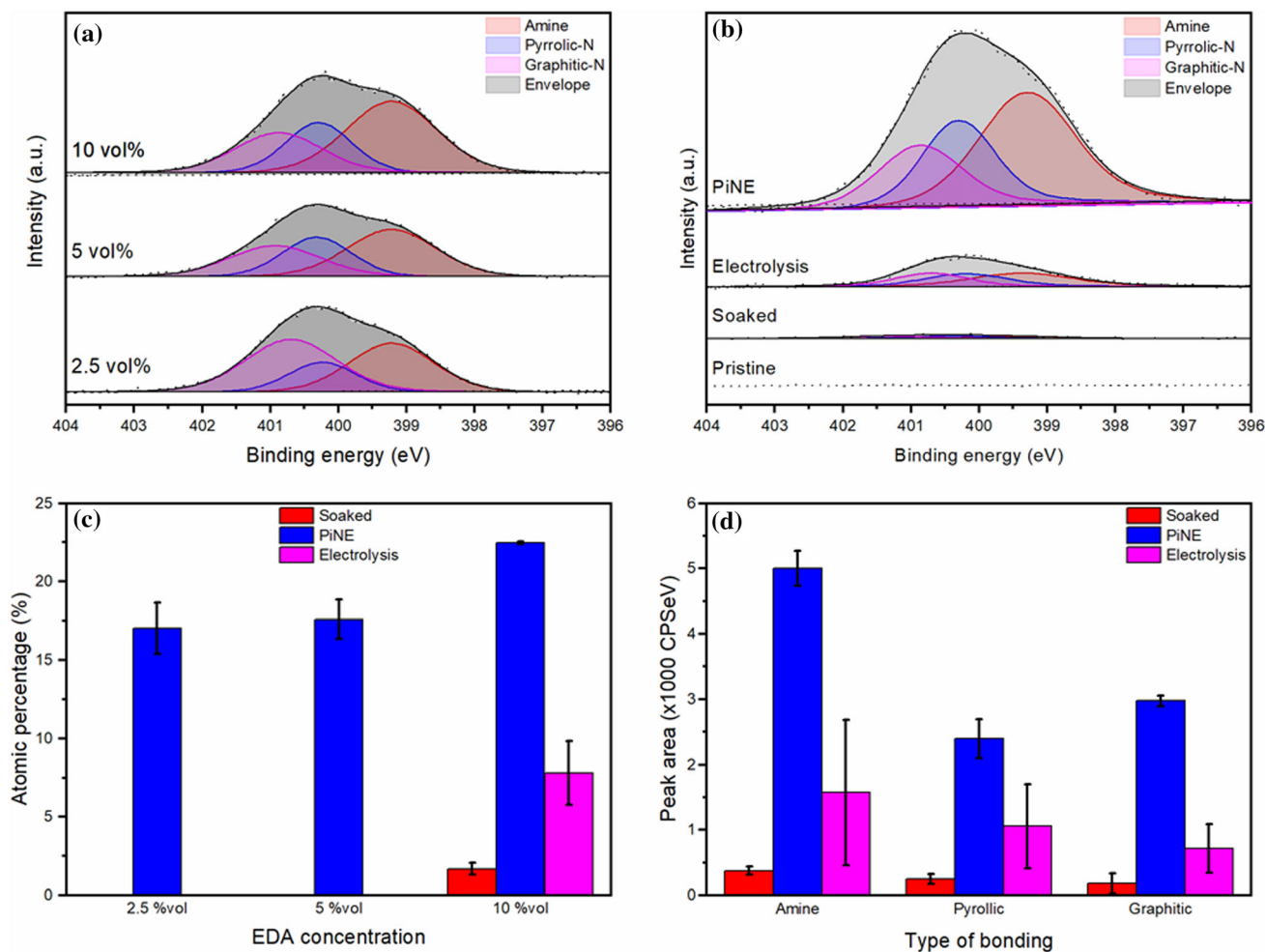


Figure 3 **a** X-ray photoelectron spectra for of N 1s high-resolution spectra for samples treated by PiNE and with ethylenediamine volume percentages of 2.5%, 5% and 10%. **b** A comparison of the nitrogen 1s peak for pristine, soaked and electrolysis treated ribbons against that for PiNE-treated samples at

10 vol% ethylenediamine. **c** The atomic percentage of nitrogen measured by X-ray photoelectron spectroscopy for samples treated in an ethylenediamine solution. **d** A comparison of the peak areas of amine, pyrrolic and graphitic nitrogen groups for soaked, PiNE and electrolysis configurations at 10 vol% EDA.

sample included demonstrating the zero nitrogen content of the untreated materials. This figure clearly illustrates that whilst the three major components are present, graphitic, amine and pyrrolic nitrogen, the peak areas are shown to be much lower in the case of soaking and electrolysis. The nitrogen content for all samples was determined based on the area under the curves using the appropriate sensitivity factors to produce atomic percentages, Fig. 3c. It is abundantly clear that the inclusion of nitrogen is greatly enhanced when the CNT ribbon is treated by PiNE. With 2.5 vol% and 5 vol% EDA, the PiNE samples yield 17 at% and 17.6 at% nitrogen, respectively. With the 10 vol% EDA electrolyte a mean value of 22.5 at% nitrogen was achieved and it is of note that this value

has surpassed the previous highest nitrogen concentration (21.26 at%) [16]. We should note that we have also tried with higher EDA concentrations (e.g. see figure S5 in the Supporting Information), however, possibly due to competing reaction mechanisms, the doping did not increase further. N-functionalization by soaking and electrolysis reached only 1.7 at% and 7.8 at%, respectively, with the same 10 vol% EDA, Fig. 3c. Further analysis of the N 1s fitted peak areas at 10 vol% EDA is presented in Fig. 3d. PiNE can be seen to give peak areas with several thousand counts per second eV (CPSeV) more than the soaked sample. The electrolysis method yields enhanced functionalization compared to the soaking at 10 vol% EDA, but

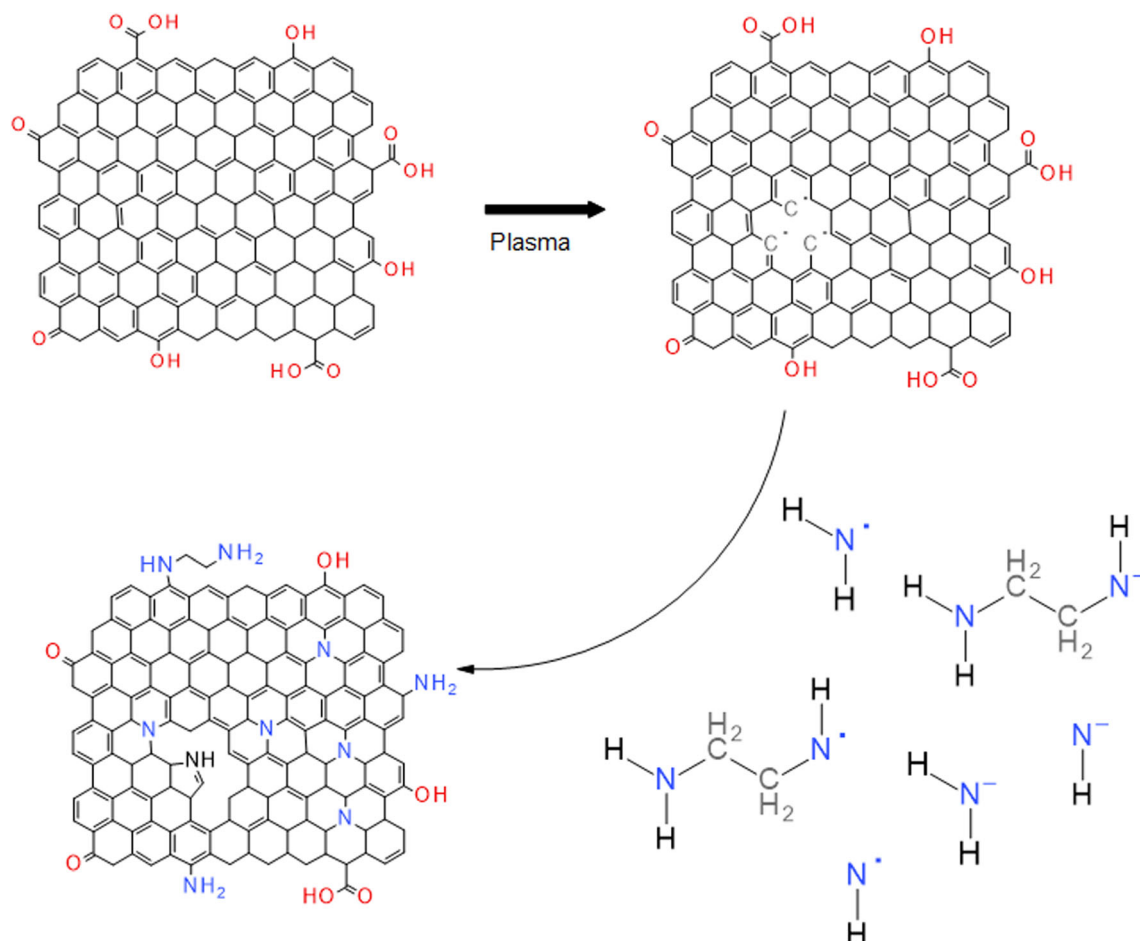


Figure 4 The plasma-liquid treatment may result in the radicalization of the graphitic lattice and the formation of additional defect sites. The generated nitrogen species may then bind to these sites to produced nitrogen-functionalized carbon nanotubes.

still falls short of the PiNE by a factor of 3.3 for amine, 2.3 for pyrrolic-N and 4.1 for the graphitic-N bonding.

In order to fully appreciate the mechanisms that lead to nitrogen incorporation in the CNTs, in depth kinetic modelling would be required as, experimentally, the generation of active species and importantly the surface reactions cannot be decoupled from the functionalization process as a whole (see below). However, our experimental results can provide the basis for some insights into the complexity of these plasma-induced chemical pathways. For instance, the differences between the plasma-based PiNE, the electrolysis methods and the other trialled configurations indicate that either the primary functionalization pathway is accelerated by the plasma-generated species or the plasma-generated species open a new reactive pathway which results in the greater degree of functionalization. As the content of nitrogen is significantly increased in the case where

the CNTs acts as the anode (electron acceptor) compared to the other configurations in the SI, negatively charged/nucleophilic nitrogen species must have an active role in the functionalization steps and can result from the electron-induced reactions at the plasma-liquid interface.

Gas-phase electrons and solvated electrons exist at high densities/concentrations above the interface and at the liquid-side of the interface, respectively, [41–43]; this is particularly true in this case where the liquid acts as the anode and are concentrated in the near-plasma region.

Electrons both in the gas phase as well as in their solvated state decompose water molecules to form a range of species including H, OH⁻ ions, OH radicals and all these have been reported to initiate hydrogen detachment of dissolved acetonitrile (C–H bond energy 413 kJ mol⁻¹) to form highly reactive free radical monomers [44]. It is therefore feasible and

reasonable to anticipate hydrogen detachment for EDA at the N–H bond terminations which have lower bond energy (391 kJ mol^{-1}) [45] than the C–H termination of acetonitrile. These hydrogen detachment reactions result in EDA radical and charged species and EDA ions may undergo further hydrogen detachment reactions and decompose into several additional species such as $\cdot\text{NH}_2$. It has been shown in the literature that these nucleophilic intermediaries of EDA (strong reducing agents) and radicals created at the plasma-liquid interface graft onto the sidewalls of a CNT/graphene by opening the carbon double-bonds [46, 47] and creating additional defects sites [44]. The combination of these defect-creating mechanisms can be used to explain the greater concentration of nitrogen functional groups achieved in this work as our experimental results confirm that higher nitrogen concentrations can be achieved when the CNTs participate as an active electrode and that electrolysis alone is unable to produce the required radical species. Figure 4 summarizes these mechanisms.

Conclusions

Nitrogen has been successfully included within the ribbon using this solution-based plasma treatment, with a dramatic increase in amine, pyrrolic and graphitic nitrogen groups, especially in the case of the ribbon electrode. In fact, we achieved an exceptionally high nitrogen concentration of 22.5 at%. This plasma-liquid treatment may present an alternative method to produce functionalized materials for industry, where the nitrogen groups added to the CNT in this work would lend themselves to a myriad of applications including, enhanced dispersion in the resins typically used for forming advanced composite materials [12], lithium storage [48], metal-free catalysis [49] and CNT photovoltaic cells [50]. The plasma-generated species are suggested to enhance the defect and carbon radicals concentrations which would aid the grafting of nitrogen groups into the lattice.

Acknowledgements

The authors would like to acknowledge the EPSRC for supporting this work through EP/M015211/1 and EP/R008841/1.

Declarations

Conflict of interest The authors declare that they have no conflict of interest.

Supplementary Information: The online version contains supplementary material available at <http://doi.org/10.1007/s10853-022-07463-7>.

Open Access This article is licensed under a Creative Commons Attribution 4.0 International License, which permits use, sharing, adaptation, distribution and reproduction in any medium or format, as long as you give appropriate credit to the original author(s) and the source, provide a link to the Creative Commons licence, and indicate if changes were made. The images or other third party material in this article are included in the article's Creative Commons licence, unless indicated otherwise in a credit line to the material. If material is not included in the article's Creative Commons licence and your intended use is not permitted by statutory regulation or exceeds the permitted use, you will need to obtain permission directly from the copyright holder. To view a copy of this licence, visit <http://creativecommons.org/licenses/by/4.0/>.

References

- [1] Lee J, Lee DM, Jung Y, Park J, Lee HS, Kim YK, Park CR, Jeong HS, Kim SM (2019) Direct spinning and densification method for high-performance carbon nanotube fibers. *Nat Commun* 10:1–10. <https://doi.org/10.1038/s41467-019-10998-0>
- [2] Li N, Huang Y, Du F, He X, Lin X, Gao H, Ma Y, Li F, Chen Y, Eklund PC (2006) Electromagnetic interference (EMI) shielding of single-walled carbon nanotube epoxy composites. *Nano Lett* 6:1141–1145. <https://doi.org/10.1021/nl0602589>
- [3] Zhou G, Wang D-W, Hou P-X, Li W, Li N, Liu C, Li F, Cheng H-M (2012) A nanosized Fe_2O_3 decorated single-walled carbon nanotube membrane as a high-performance flexible anode for lithium ion batteries. *J Mater Chem* 22:17942. <https://doi.org/10.1039/c2jm32893c>
- [4] Ban C, Wu Z, Gillaspie DT, Chen L, Yan Y, Blackburn JL, Dillon AC (2010) Nanostructured Fe_3O_4 /SWNT electrode: binder-free and high-rate li-ion anode. *Adv Mater* 22:E145–E149. <https://doi.org/10.1002/adma.200904285>

- [5] Zhang H, Wang Y, Zhao W, Zou M, Chen Y, Yang L, Xu L, Wu H, Cao A (2017) MOF-derived ZnO nanoparticles covered by N-doped carbon layers and hybridized on carbon nanotubes for lithium-ion battery anodes. *ACS Appl Mater Interfaces* 9:37813–37822. <https://doi.org/10.1021/acsami.7b12095>
- [6] Zhou RW, Zhou RS, Zhuang JX, Li JW, Chen MD, Zhang XH, Liu DP, Ostrikov KK, Yang SZ (2016) Surface diffuse discharge mechanism of well-aligned atmospheric pressure microplasma arrays. *Chinese Phys B* 25:045202. <https://doi.org/10.1088/1674-1056/25/4/045202>
- [7] Mallakpour S, Soltanian S (2016) Surface functionalization of carbon nanotubes: fabrication and applications. *RSC Adv* 6:109916–109935. <https://doi.org/10.1039/c6ra24522f>
- [8] Gorji TB, Ranjbar AA, Mirzababaei SN (2015) Optical properties of carboxyl functionalized carbon nanotube aqueous nanofluids as direct solar thermal energy absorbers. *Sol Energy* 119:332–342. <https://doi.org/10.1016/j.solener.2015.07.012>
- [9] Karami M, Akhavan Bahabadi MAA, Delfani S, Ghozatloo A (2014) A new application of carbon nanotubes nanofluid as working fluid of low-temperature direct absorption solar collector. *Sol Energy Mater Sol Cells* 121:114–118. <https://doi.org/10.1016/j.solmat.2013.11.004>
- [10] Yellapu G, Chachin Vishal CV, Kandoth MP, Saha P, Bojja RR, Gandham S, Kanaparthi R (2019) Functionalized multi-walled carbon nanotubes based Newtonian Nano fluids for medium temperature heat transfer applications. *Therm Sci Eng Prog* 12:100350. <https://doi.org/10.1016/j.tsep.2019.04.014>
- [11] Mesgari S, Hjerrild N, Arandiyan H, Taylor RA (2018) Carbon nanotube heat transfer fluids for solar radiant heating of buildings. *Energy Build* 175:11–16. <https://doi.org/10.1016/j.enbuild.2018.07.002>
- [12] Jung H, Choi HK, Kim S, Lee H-S, Kim Y, Yu J (2017) The influence of N-doping types for carbon nanotube reinforced epoxy composites: a combined experimental study and molecular dynamics simulation. *Compos Part A Appl Sci Manuf* 103:17–24. <https://doi.org/10.1016/j.compositesa.2017.09.005>
- [13] Williams J, Broughton W, Koukoulas T, Rahatekar SS (2013) Plasma treatment as a method for functionalising and improving dispersion of carbon nanotubes in epoxy resins. *J Mater Sci* 48:1005–1013. <https://doi.org/10.1007/s10853-012-6830-3>
- [14] Hulicova-Jurcakova D, Seredych M, Lu GQ, Bandosz TJ (2009) Combined effect of nitrogen- and oxygen-containing functional groups of microporous activated carbon on its electrochemical performance in supercapacitors. *Adv Funct Mater* 19:438–447. <https://doi.org/10.1002/adfm.200801236>
- [15] Thirumal V, Pandurangan A, Jayavel R, Krishnamoorthi SR, Ilangovan R (2016) Synthesis of nitrogen doped coiled double walled carbon nanotubes by chemical vapor deposition method for supercapacitor applications. *Curr Appl Phys* 16:816–825. <https://doi.org/10.1016/j.cap.2016.04.018>
- [16] Hussain S, Amade R, Jover E, Bertran E (2013) Nitrogen plasma functionalization of carbon nanotubes for supercapacitor applications. *J Mater Sci* 48:7620–7628. <https://doi.org/10.1007/s10853-013-7579-z>
- [17] Yin L-C, Liang J, Zhou G-M, Li F, Saito R, Cheng H-M (2016) Understanding the interactions between lithium polysulfides and N-doped graphene using density functional theory calculations. *Nano Energy* 25:203–210. <https://doi.org/10.1016/j.nanoen.2016.04.053>
- [18] Zuo P, Zhang H, He M, Li Q, Ma Y, Du C, Cheng X, Huo H, Gao Y, Yin G (2017) Clew-like N-doped multiwalled carbon nanotube aggregates derived from metal-organic complexes for lithium-sulfur batteries. *Carbon N Y* 122:635–642. <https://doi.org/10.1016/j.carbon.2017.07.017>
- [19] Inagaki M, Toyoda M, Soneda Y, Morishita T (2018) Nitrogen-doped carbon materials. *Carbon N Y* 132:104–140. <https://doi.org/10.1016/j.carbon.2018.02.024>
- [20] Qu L, Liu Y, Baek J-B, Dai L (2010) Nitrogen-doped graphene as efficient metal-free electrocatalyst for oxygen reduction in fuel cells. *ACS Nano* 4:1321–1326. <https://doi.org/10.1021/nn901850u>
- [21] Gong K, Du F, Xia Z, Durstock M, Dai L (2009) Nitrogen-doped carbon nanotube arrays with high electrocatalytic activity for oxygen reduction. *Science* 323:760–764. <https://doi.org/10.1126/science.1168049>
- [22] Te Hsieh C, Teng H, Chen WY, Cheng YS (2010) Synthesis, characterization, and electrochemical capacitance of amino-functionalized carbon nanotube/carbon paper electrodes. *Carbon N Y* 48:4219–4229. <https://doi.org/10.1016/j.carbon.2010.07.021>
- [23] Narwade SS, Mali SM, Sathe BR (2021) Amine-functionalized multi-walled carbon nanotubes (EDA-MWCNTs) for electrochemical water splitting reactions. *New J Chem* 45:3932–3939. <https://doi.org/10.1039/d0nj05479h>
- [24] Arjmand M, Chizari K, Krause B, Pötschke P, Sundararaj U (2016) Effect of synthesis catalyst on structure of nitrogen-doped carbon nanotubes and electrical conductivity and electromagnetic interference shielding of their polymeric nanocomposites. *Carbon N Y* 98:358–372. <https://doi.org/10.1016/j.carbon.2015.11.024>
- [25] Arjmand M, Sundararaj U (2015) Electromagnetic interference shielding of nitrogen-doped and undoped carbon nanotube/polyvinylidene fluoride nanocomposites: a comparative study. *Compos Sci Technol* 118:257–263. <https://doi.org/10.1016/j.compscitech.2015.09.012>

- [26] John AR, Arumugam P (2015) Open ended nitrogen-doped carbon nanotubes for the electrochemical storage of energy in a supercapacitor electrode. *J Power Sour* 277:387–392. <https://doi.org/10.1016/j.jpowsour.2014.11.151>
- [27] Kanygin MA, Sedelnikova OV, Asanov IP, Bulusheva LG, Okotrub AV, Kuzhir PP, Plyushch AO, Maksimenko SA, Lapko KN, Sokol AA, Ivashkevich OA, Lambin P (2013) Effect of nitrogen doping on the electromagnetic properties of carbon nanotube-based composites. *J Appl Phys*. <https://doi.org/10.1063/1.4800897>
- [28] Aguilar-Elguézabal A, Román-Aguirre M, De la Torre L, Zaragoza EA (2017) Acrylonitrile, an advantageous precursor to synthesize nitrogen doped carbon nanotubes. *J Phys Chem Solids* 104:52–55. <https://doi.org/10.1016/j.jpics.2016.12.023>
- [29] Sharma A, Dasgupta K, Patwardhan A, Joshi J (2017) Kinetic study of nitrogen doped carbon nanotubes in a fixed bed. *Chem Eng Sci* 170:756–766. <https://doi.org/10.1016/j.ces.2017.03.017>
- [30] Soares OSGP, Rocha RP, Gonçalves AG, Figueiredo JL, Órfão JJM, Pereira MFR (2015) Easy method to prepare N-doped carbon nanotubes by ball milling. *Carbon N Y* 91:114–121. <https://doi.org/10.1016/j.carbon.2015.04.050>
- [31] Liu Y, Shen Y, Sun L, Li J, Liu C, Ren W, Li F, Gao L, Chen J, Liu F, Sun Y, Tang N, Cheng HM, Du Y (2016) Elemental superdoping of graphene and carbon nanotubes. *Nat Commun*. <https://doi.org/10.1038/ncomms10921>
- [32] Vlad I-E, Anghel SD (2017) Time stability of water activated by different on-liquid atmospheric pressure plasmas. *J Electrostat* 87:284–292. <https://doi.org/10.1016/j.elstat.2017.06.002>
- [33] Carolan D, Rocks C, Padmanaban DB, Maguire P, Svrcek V, Mariotti D (2017) Environmentally friendly nitrogen-doped carbon quantum dots for next generation solar cells, *Sustain. Energy Fuels* 1:1611–1619. <https://doi.org/10.1039/C7SE00158D>
- [34] Dsouza SD, Buerkle M, Brunet P, Maddi C, Padmanaban DB, Morelli A, Payam AF, Maguire P, Mariotti D, Svrcek V (2021) The importance of surface states in N-doped carbon quantum dots. *Carbon N Y* 183:1–11. <https://doi.org/10.1016/j.carbon.2021.06.088>
- [35] Li YL, Kinloch IA, Windle AH (2004) Direct spinning of carbon nanotube fibers from chemical vapor deposition synthesis. *Science* 304:276–278. <https://doi.org/10.1126/science.1094982>
- [36] Brunet P, McGlynn RJ, Alessi B, Smail F, Boies A, Maguire P, Mariotti D (2021) Surfactant-free synthesis of copper nanoparticles and gas phase integration in CNT-composite materials. *Nanoscale Adv* 3:781–788. <https://doi.org/10.1039/d0na00922a>
- [37] Weller L, Smail FR, Elliott JA, Windle AH, Boies AM, Hochgreb S (2019) Mapping the parameter space for direct-spun carbon nanotube aerogels. *Carbon N Y* 146:789–812. <https://doi.org/10.1016/j.carbon.2019.01.091>
- [38] Chakrabarti S, Kume H, Pan L, Nagasaka T, Nakayama Y (2007) Number of walls controlled synthesis of millimeter-long vertically aligned brushlike carbon nanotubes. *J Phys Chem C* 111:1929–1934. <https://doi.org/10.1021/jp0666986>
- [39] Sundaram RM, Koziol KKK, Windle AH (2011) Continuous direct spinning of fibers of single-walled carbon nanotubes with metallic chirality. *Adv Mater* 23:5064–5068. <https://doi.org/10.1002/adma.201102754>
- [40] Miao M (2011) Electrical conductivity of pure carbon nanotube yarns. *Carbon N Y* 49:3755–3761. <https://doi.org/10.1016/j.carbon.2011.05.008>
- [41] Richmonds C, Witzke M, Bartling B, Lee SW, Wainright J, Liu C-C, Sankaran RM (2011) Electron-transfer reactions at the plasma-liquid interface. *J Am Chem Soc* 133:17582–17585. <https://doi.org/10.1021/ja207547b>
- [42] Rumbach P, Witzke M, Sankaran RM, Go DB (2013) Decoupling interfacial reactions between plasmas and liquids: charge transfer versus plasma neutral reactions. *J Am Chem Soc* 135:16264–16267. <https://doi.org/10.1021/ja407149y>
- [43] Rumbach P, Bartels DM, Go DB (2018) The penetration and concentration of solvated electrons and hydroxyl radicals at a plasma-liquid interface. *Plasma Sour Sci Technol* 27:115013. <https://doi.org/10.1088/1361-6595/aaed07>
- [44] Senthilnathan J, Rao KS, Yoshimura M (2014) Submerged liquid plasma-low energy synthesis of nitrogen-doped graphene for electrochemical applications. *J Mater Chem A* 2:3332–3337. <https://doi.org/10.1039/c3ta14946c>
- [45] Zumdahl SS, Zumdahl SA (2000) *Chemistry*. Houghton Mifflin, Boston
- [46] Gromov AV, Gray N, Szilágyi PÁ, Campbell EEB (2012) Direct grafting of carbon nanotubes with ethylenediamine. *J Mater Chem* 22:21242–21248. <https://doi.org/10.1039/c2jm33348a>
- [47] Wang S, Wang J, Zhang W, Ji J, Li Y, Zhang G, Zhang F, Fan X (2014) Ethylenediamine modified graphene and its chemically responsive supramolecular hydrogels. *Ind Eng Chem Res* 53:13205–13209. <https://doi.org/10.1021/ie501448p>
- [48] Shin WH, Jeong HM, Kim BG, Kang JK, Choi JW (2012) Nitrogen-doped multiwall carbon nanotubes for lithium storage with extremely high capacity. *Nano Lett* 12:2283–2288. <https://doi.org/10.1021/nl3000908>
- [49] Tuci G, Zafferoni C, Rossin A, Milella A, Luconi L, Innocenti M, Truong Phuoc L, Duong-Viet C, Pham-Huu C, Giambastiani G (2014) Chemically functionalized carbon

nanotubes with pyridine groups as easily tunable N-decorated nanomaterials for the oxygen reduction reaction in alkaline medium. *Chem Mater* 26:3460–3470. <https://doi.org/10.1021/cm500805c>

- [50] Kalita G, Adhikari S, Aryal HR, Afre R, Soga T, Sharon M, Umeno M (2009) Functionalization of multi-walled carbon nanotubes (MWCNTs) with nitrogen plasma for photovoltaic

device application. *Curr Appl Phys* 9:346–351. <https://doi.org/10.1016/j.cap.2008.03.007>

Publisher's Note Springer Nature remains neutral with regard to jurisdictional claims in published maps and institutional affiliations.